JCI The Journal of Clinical Investigation

Sialic acid is a critical fetal defense against maternal complement attack

Markus Abeln, Iris Albers, Ulrike Peters-Bernard, Kerstin Flächsig-Schulz, Elina Kats, Andreas Kispert, Stephen Tomlinson, Rita Gerardy-Schahn, Anja Münster-Kühnel, Birgit Weinhold

J Clin Invest. 2018. https://doi.org/10.1172/JCI99945.

Research In-Press Preview **Immunology** **Reproductive biology**

The negatively charged sugar sialic acid (Sia) occupies the outermost position in the bulk of cell surface glycans. Lack of sialylated glycans due to genetic ablation of the Sia activating enzyme CMP-sialic acid synthase (CMAS) resulted in embryonic lethality around day 9.5 post coitum (E9.5) in mice. Developmental failure was caused by complement activation on trophoblasts in $Cmas^{-/-}$ implants accompanied by infiltration of maternal neutrophils at the fetal-maternal interface, intrauterine growth restriction, impaired placental development and a thickened Reichert's membrane. This phenotype, which shared features with complement-recepter-1 related protein Y (Crry) depletion, was rescued in E8.5 $Cmas^{-/-}$ mice upon injection of cobra venom factor resulting in exhaustion of the maternal complement component C3. Here we show that Sia is dispensable for early development of the embryo proper, but pivotal for fetal-maternal immune homeostasis during pregnancy, i.e. for protecting the allograft implant against attack by the maternal innate immune system. Finally, embryos devoid of cell surface sialylation suffered from malnutrition due to inadequate placentation as secondary effect.

Sialic acid is a critical fetal defense against maternal complement attack

Markus Abeln[1], Iris Albers[1], Ulrike Peters-Bernard[1], Kerstin Flächsig-Schulz[1], Elina Kats[1], Andreas Kispert[2], Stephen Tomlinson[3], Rita Gerardy-Schahn[1], Anja Münster-Kühnel[1], Birgit Weinhold[1]

[1]Institut for Clinical Biochemistry, Hannover Medical School, 30625 Hannover, Germany

[2]Institut for Molecular Biology, Hannover Medical School, 30625 Hannover, Germany

[3]Department of Microbiology and Immunology, Children's Research Institute, Medical University of South Carolina, Charleston, SC 29425, USA

The authors have declared that no conflict of interest exists.

Corresponding authors:

Birgit Weinhold, Institut für Klinische Biochemie, Medizinische Hochschule Hannover, Carl-Neuberg-Strasse 1, 30625 Hannover, Germany
Phone: +49511-5323947
Weinhold.Birgit@mh-hannover.de

Anja Münster-Kühnel, Institut für Klinische Biochemie, Medizinische Hochschule Hannover, Carl-Neuberg-Strasse 1, 30625 Hannover, Germany
Phone: +49511-5323947
Muenster.Anja@mh-hannover.de

Abstract:

The negatively charged sugar sialic acid (Sia) occupies the outermost position in the bulk of cell surface glycans. Lack of sialylated glycans due to genetic ablation of the Sia activating enzyme CMP-sialic acid synthase (CMAS) resulted in embryonic lethality around day 9.5 post coitum (E9.5) in mice. Developmental failure was caused by complement activation on trophoblasts in *Cmas*$^{-/-}$ implants accompanied by infiltration of maternal neutrophils at the fetal-maternal interface, intrauterine growth restriction, impaired placental development and a thickened Reichert's membrane. This phenotype, which shared features with complement-recepter-1 related protein Y (Crry) depletion, was rescued in E8.5 *Cmas*$^{-/-}$ mice upon injection of cobra venom factor resulting in exhaustion of the maternal complement component C3. Here we show that Sia is dispensable for early development of the embryo proper, but pivotal for fetal-maternal immune homeostasis during pregnancy, i.e. for protecting the allograft implant against attack by the maternal innate immune system. Finally, embryos devoid of cell surface sialylation suffered from malnutrition due to inadequate placentation as secondary effect.

INTRODUCTION

Every living cell is coated with a dense layer of glycans, the glycocalyx. In mammals, ten different monosaccharides can be assembled in various linkages, generating an enormous number of glycans, encoding a vast amount of information which is utilized in cellular communication (1). Moreover, glycosylation of proteins and lipids is cell-type-specific and influenced by e.g. metabolic state, differentiation and environmental factors (2). Although recent advances in glycoanalytical technologies now shed light on specific glycosylation patterns and identify disease-associated alterations, many structure-function relationships still await elucidation (3). A sugar known to have a major impact on the functions of glycans is the negatively charged nonulose sialic acid (Sia). Sia is situated at the terminal position of a multitude of glycan structures, thus shaping the outermost identity of a cell. It is therefore not surprising that Sia modulates central cellular functions such as cell-cell communication, signal transduction, and cell migration (3,4). Moreover, Sia can dampen immune responses by acting as a ligand for Sia-binding immunoglobulin-like lectins (Siglecs), predominantly found on immune cells, and the complement regulating fluid-phase protein factor H (5,6). Hence, Sia is recognized as self-associated molecular patterns (SAMP), promoting discrimination between self and non-self (7). Sialylation in mammals occurs in either α2,3- or α2,6- glycosidic linkage to the underlying sugar galactose or *N*-acetylgalactosamine, or in an α2,8-linkage when two or more Sia residues are linked to another in di-, oligo- or polysialylated glycans by Golgi-resident sialyltransferases. All sialyltransferases strictly depend on the preceding activation of Sia to CMP-Sia, which is catalysed by the nuclear localised enzyme CMP-sialic acid synthase (CMAS) (8). We have recently shown that genetic inactivation of the *Cmas* gene results in loss of CMAS protein and complete lack of sialoglycans on the cell surface of murine embryonic stem cells (mESC) (9). Fully unexpectedly, the asialo mESC were equivalent to control mESC in terms of differentiation, indicating that Sia is dispensable for germ layer formation and early embryonic development in vitro. In accord with our observations, a mouse model deficient in the first committed enzyme in the Sia de novo biosynthesis, the bifunctional enzyme UDP-*N*-acetylglucosamine 2-epimerase/*N*-acetylmannosamine kinase (GNE), is embryonic lethal around E9.5, a time point when all germ layers have formed (10). Nevertheless, the embryonic lethal GNE phenotype highlights the substantial importance of Sia for mammalian development.

In eutherian pregnancy exact orchestration of signalling events and precise immune homeostasis are crucial for proper development and survival of the fetus (11). During early pregnancy, the blastocyst stage embryo is subdivided into the inner cell mass, giving rise to the embryo proper, and the trophoblast layer, forming extraembryonic tissues from which amongst others the future placenta derives (12). However, also the inner cell mass contributes to the generation of extraembryonic tissues by forming the Reichert's membrane and the visceral endoderm, which ensure fetal nourishment during early development until blood flow through the placenta is properly established at E14.5 in mice (13-15). Evolution established different types of placentation in mammals. Mice and humans both form a hemochorial placenta, in which the maternal blood passes through vascular spaces with fetal trophoblast cells, rather than maternal endothelial cells forming the vascular barrier (16). Consequently, the extraembryonic components of the developing fetus are in direct contact to maternal blood. This is a challenging situation since the embryo bears paternal antigens and is a semi-allograft to its mother. Thus, fetal trophoblasts in hemochorial placentae are particularly vulnerable and in need of preventing an immune attack at the fetal-maternal interface. Numerous immune protective mechanisms have evolved to fulfil this task. On the fetal side for instance, trophoblasts express a distinct subset of MHC molecules that seem to promote maternal immune tolerance of fetal tissues (17-19). Additionally, multiple complement regulatory proteins (CD55, CD46, CD59 and Crry) are expressed on fetal trophoblasts and control first line immune defence mechanisms (20,21). On the maternal side, the decidua protects the developing embryo by limiting access of maternal T- and B-cells to the implant (22,23). Dysregulation of immune homeostasis during pregnancy can lead to severe complications, such as recurrent pregnancy loss or preeclampsia. The latter affects 2-8% of pregnancies

worldwide and patients show placental deficits and intrauterine growth restriction, hence posing a severe threat for mother and fetus (24-26).

Although Sia is known for long as pivotal for embryonic development and involved in immunoregulation, its precise functions and its role in the interplay between immune protection and embryonic development in mammals is not understood so far. Here, we demonstrate that sialylation is less important for early developmental steps of the embryo proper, but is crucial for maintenance of immune-homeostasis at the fetal-maternal interface. Trophoblasts were extensively sialylated in the wildtype, but did not express Sia in *Cmas*$^{-/-}$ embryos. As a consequence immune-protection failed and the maternal complement system attacked extraembryonic tissues resulting in defective placentation, intrauterine growth restriction and ultimately fetal demise.

RESULTS

Depletion of CMAS leads to loss of sialoglycoconjugates in *Cmas*$^{-/-}$ embryos and is embryonic lethal

Genetic inactivation of *Cmas* in mice was accomplished as described by excision of exon 4, which encodes residues essential for enzymatic activity (9). All genotypes of offspring from *Cmas*$^{+/-}$ intercrosses were discovered in Mendelian ratio until E8.5 (Figure S1). *Cmas*$^{-/-}$ embryos were observed only very rarely between E9 and E10 and were never born. *Cmas* heterozygous mice were indistinguishable from wildtype. To evaluate the sialylation pattern in control and *Cmas*$^{-/-}$ E6.5 and E8.5 implants, paraffin sections from uteri of pregnant *Cmas*$^{+/-}$ female (bred to *Cmas*$^{+/-}$ males) were stained with *Maackia amurensis* agglutinin (MAA), which binds to α2,3-linked sialic acids on glycans (Figure 1A). Simultaneously, the same sections were probed with peanut agglutinin (PNA) lectin, detecting galactose as terminal sugar (27). Since under normal conditions the bulk of galactose residues is capped with Sia, PNA staining becomes prominent in the absence of Sia (Figure 1A). In E6.5 control animals, MAA reactivity was prominent on the surface of trophoblast cells at the ectoplacental cone (EPC), on trophoblast giant cells (TGC) lining the fetal-maternal interface (arrowheads) and on the apical side of the embryonic and extraembryonic ectoderm facing the proamniotic cavity (arrow) (Figure 1B). Notably, apart from the observed reactivity at the apical side of the embryonic ectoderm, the embryo proper did not exhibit MAA reactivity. At E8.5, MAA reactivity at the EPC and on TGC became even more pronounced and could also be observed on the Reichert's membrane (asterisk), head mesenchymal cells (arrowheads) and the apical side of fetal epithelia (arrows) in control animals. TGC identity of MAA positive cells at the fetal-maternal interface of control implants was verified by co-staining of MAA and the trophoblast marker cytokeratin-8 (Figure S2A). Consistent with *Cmas*$^{-/-}$ mESC, E6.5 as well as E8.5 *Cmas*$^{-/-}$ embryonic and extraembryonic tissues were devoid of α2,3-linked sialic acids as visualized by lack of MAA staining. The MAA positive cells in the vicinity of *Cmas* negative TGCs have been identified as maternal granulocytes (Figure S2B). To confirm the loss of Sia on glycans and in order to detect terminal galactose residues, uteri sections were simultaneously probed with PNA. Control animals showed slight PNA reactivity at the apical side of epithelia at E6.5 and E8.5 (Figure 1B, arrows), whereas *Cmas*$^{-/-}$ tissue was highly PNA positive with particularly intense staining in the trophoblast layer and at the apical side of visceral endoderm cells at both analysed time points. Hence, loss of terminal Sia resulted in concomitant appearance of underlying galactosyl residues on the cell surface of *Cmas*$^{-/-}$ embryonic and extraembryonic tissues. Interestingly, the PNA staining in *Cmas*$^{-/-}$ trophoblasts resembled the pattern of MAA staining in control animals, suggesting that most of the PNA epitopes on control trophoblasts were capped with α2,3-linked sialic acids. Specificity of the MAA reactivity for Sia was confirmed by enzymatic removal of Sia by neuraminidase treatment of the sections prior to incubation with the lectins. As expected, neuraminidase treatment abolished MAA staining in control animals and gave rise to PNA staining on trophoblasts, embryonic epithelia and mesenchymal cells. Neuraminidase treated *Cmas*$^{-/-}$ tissues did not show any difference in MAA or PNA reactivity compared to untreated samples of the same genotype (Figure 1B). Visualisation of α2,6-linked sialic acids was accomplished by detection with *Sambucus nigra* agglutinin (SNA). SNA reactivity was prominent on the cell surface of embryonic ectodermal cells (arrow) as well as on amniotic and allantoic cells in control embryos (Figure S3). In addition, TGCs showed an intracellular staining for SNA. *Cmas*$^{-/-}$ implants lacked cell surface SNA reactivity of the aforementioned tissues, but like wildtype displayed the intracellular SNA staining in TGCs, which most likely reflects endocytosed material of maternal origin. The Sia specificity of the lectin was again demonstrated by complete loss of SNA reactivity and an increase in PNA epitopes upon enzymatic removal of Sia by neuraminidase treatment prior to lectin incubation. The simultaneous lack of MAA and SNA reactivity and the presence of PNA binding sites in knockout embryos confirmed that loss of CMAS activity resulted in a complete lack of cell surface sialylation referred to as asialo phenotype, identical to the situation in *Cmas*$^{-/-}$ mESCs (9).

Loss of CMAS results in intrauterine growth restriction

To follow up embryonic development hematoxylin and eosin stained sections of uteri were assessed. At E6.5 the morphology of embryonic ectoderm (EC) and extraembryonic ectoderm, visceral endoderm (VE) and the proamniotic cavity (PC) was indistinguishable between *Cmas*$^{-/-}$ and control implants (Figure 2A). At E7.5 the three germlayers ectoderm, endoderm, and mesoderm (ME) had been established in control as well as *Cmas*$^{-/-}$ embryos. Mesodermal cells could be observed migrating from the primitive streak to the anterior part of the embryo in both genotypes (Figure 2A, insets). At E8.5, *Cmas*$^{-/-}$ mice were characterised by a marked variability in developmental deficits. Some embryos formed somites (S), the heart (H) and showed neurulation, whereas others were considerably less well-structured or consisted of a widely unstructured agglomeration of cells (Figure 2A and S4A). Phenotypic variability was also reflected by heterogeneous organisation of mesodermal structures, which we monitored by in situ hybridisation analysis of the major mesoderm regulator *brachyury*. *Brachyury* was localised at the primitive streak in control animals but was either irregularly distributed or ectopically expressed in numerous *Cmas*$^{-/-}$ embryos (Figure S4B). To quantify the fetal growth between E6.5 and E8.5, the combined total area of amniotic cavity, exocoelomic cavity, ectoplacental cavity and embryo proper was measured on sagittal sections. A schematic overview is depicted in Figure S5. At E6.5 no significant differences in fetal growth were observed (Figure 2B). At E7.5, *Cmas*$^{-/-}$ mice showed only 52% ($p = 0.045$) of the size of control animals (*Cmas*$^{+/+}$ or *Cmas*$^{+/-}$). Intrauterine growth restriction (IUGR) increased with progression of pregnancy at E8.5, where *Cmas*$^{-/-}$ embryos reached only 36% ($p = 0.029$) of the size of controls. Taken together, loss of sialylation did not impair morphogenesis and differentiation processes in the embryo proper of *Cmas*$^{-/-}$ mice until E7.5, although already a significant IUGR was observed. Growth restriction affected all *Cmas*$^{-/-}$ embryos at E8.5 and development of the embryo proper was at this time point characterized by a large variability, ranging from proper formation of e.g. somites up to embryos with extensive loss of developmental orchestration.

Cmas$^{-/-}$ mice exhibit severe extraembryonic defects

The pronounced IUGR in *Cmas*$^{-/-}$ animals together with a broad heterogeneity in the development of the embryo proper suggested a contribution of deficits in extraembryonic tissues. These tissues (e.g. visceral endoderm, amnion and trophoblasts) are embryonic derivatives that do mostly not contribute to the later animal but are essential for fetal nourishment, waste exchange, and protection. We first analysed the structure of the ectoplacental cone (EPC) and the chorionic plate (CP). Both structures harbour trophoblast stem cells, which give rise to different cell types of the later placenta (28). The EPC however is in direct contact with the maternal decidua, whereas the CP is located inside the fetal compartment at the mesometrial side of the exocoelomic cavity. Trophoblasts are characterized by expression of the intermediate filament cytokeratin-8 that could immunohistochemically be detected by the TROMA-I antibody on trophoblasts at the EPC and on trophoblast giant cells (TGC), which, due to their polyploid nature, are characterised by large nuclei (29) (Figure 2C). As described in literature, EPCs of control mice were properly structured at E8.5 and displayed internally localised trophoblast cells (arrowheads), which are reported to contribute to the spongiotrophoblast and labyrinth placental layer at later time points in development (28). In contrast, the EPC of *Cmas*$^{-/-}$ animals appeared heavily disorganised. The structure was either devoid of internally localised trophoblasts or the number of trophoblasts was dramatically decreased (Figure 2C). In addition to their localization at the EPC, TGCs continuously lined the fetal-maternal interface of control mice at the site of decidual contact. Although TGCs were present in this compartment, a continuous trophoblast layer was not established at the interface of *Cmas*$^{-/-}$ mice (Figure 2C). Importantly, the chorionic plate was properly established at E8.5 in control animals, but was absent or - in those rare cases where it could be detected in *Cmas*$^{-/-}$ mice - was dramatically reduced in its spatial expansion (Figure 2C and Figure S4A).

Another tissue important for regulation of nutrient and waste exchange during the first days of gestation when in- and efflux through the placenta is not yet established, is the Reichert's membrane (RM) (30,31). The RM is the outermost basement membrane deposited by cells of the parietal endoderm (extraembryonic tissue) and characterized by collagen IV and laminin expression. Staining of both markers in control mice showed a thin and

well-structured RM with a monolayer of parietal endoderm cells situated like pearls on a string on top, whereas *Cmas*$^{-/-}$ mice exhibited tremendous deposition of collagen IV and laminin at the RM accompanied by accumulation of parietal endodermal cells at the antimesometrial pole at E.8.5 (Figure 2D).

In sum, loss of sialylation led to the appearance of severe extraembryonic defects, which all are likely to contribute to the observed growth restriction of *Cmas*$^{-/-}$ embryos.

The fetal-maternal interface of *Cmas*$^{-/-}$ mice is infiltrated with maternal neutrophils

The detailed analysis of trophoblasts and the RM revealed that the fetal-maternal interface of *Cmas*$^{-/-}$ mice was tremendously infiltrated with polymorphonuclear leukocytes, indicating a major inflammation at the site of implantation. To investigate the immunological situation in more detail, we analysed the presence of different leukocyte populations in the decidua of *Cmas*$^{-/-}$ and control animals over time (E6.5 to E8.5). Both, neutrophils and monocytes are characterised by the granulocyte receptor-1 (Gr-1) epitope, but neutrophils can morphologically be distinguished from monocytes by segmented nuclei. At all analysed time points, Gr-1 positive cells in control mice were rare and their presence predominantly restricted to the site of contact between the EPC and the decidua (Figure 3A). However, in deciduae of *Cmas*$^{-/-}$ embryos numbers of Gr-1 positive cells were already significantly elevated up to 6-fold ($p = 0.002$) at E6.5. This increase was maintained at E7.5 ($p = 0.0001$) and dramatically augmented at E8.5 ($p = 0.002$), when the entire implantation site of *Cmas*$^{-/-}$ embryos was infiltrated with maternal neutrophils. Neutrophil identity of Gr-1 positive cells in the deciduae was verified by staining of the neutrophil specific epitope Ly6G (Figure S6). Under normal conditions, the most abundant decidual leukocyte population are decidual NK (dNK) cells, which play an important role during vascularisation and in immune surveillance in the decidua (32). dNK cells are characterized by glycoprotein rich cytoplasmic granules containing α-linked N-acetylgalactosamine, a sugar moiety that can be recognized by *Dolichus biflorus* lectin (DBA) (33). The localisation of DBA positive dNK cells was comparable in control and *Cmas*$^{-/-}$ implants from E6.5 to E8.5. Similarly, the number of DBA positive cells in the decidua basalis did not differ significantly (E6.5: $p = 0.77$; E7.5: $p = 0.112$; E8.5: $p = 0.865$) between *Cmas*$^{-/-}$ and controls (Figure 3B). Likewise, the number of decidual macrophages, identified by immunohistochemical staining of the marker F4/80, although increased at E8.5, did not deviate significantly between *Cmas*$^{-/-}$ and controls in the analysed time frame (E6.5 $p = 0.678$; E7.5 $p = 0.532$; E8.5 $p = 0.188$) (Figure 3C). We conclude that maternal neutrophils, but not decidual macrophages or dNK cells, infiltrated the fetal-maternal interface of *Cmas*$^{-/-}$ implants as early as E6.5, i.e. prior to morphological defects of *Cmas*$^{-/-}$ embryos.

Depletion of maternal neutrophils does not ameliorate the *Cmas*$^{-/-}$ phenotype

Neutrophil infiltration of the fetal-maternal interface has previously been described to contribute to fetal demise in inflammation related mouse models of recurrent pregnancy loss (24). With the aim to rescue a putative neutrophil driven inflammation and to attenuate the *Cmas*$^{-/-}$ phenotype, we injected the neutrophil specific anti-Ly6G antibody into *Cmas*$^{+/-}$ pregnant mice at day E4.5 as previously described by Daley et al. (34). To validate the absence of neutrophils in the maternal circulation after antibody treatment, maternal whole blood was analysed for Ly6G positive cells at day E8.5 by FACS analysis. The blood of untreated *Cmas*$^{+/-}$ mice harboured a distinct Ly6G positive population, which was successfully depleted in anti-Ly6G injected mice (Figure 4A). In line with depletion of neutrophils in the maternal circulation, also the prominent infiltration of *Cmas*$^{-/-}$ implants with maternal neutrophils was abolished at E8.5 (Figure 4B). However, despite the fact that neutrophilia was abrogated, *Cmas*$^{-/-}$ embryos still revealed a significant IUGR ($p = 0.0012$) similar to *Cmas*$^{-/-}$ embryos of untreated mothers (Figure 4C, Figure 2B). Moreover, the deficits in placental development, as can be seen by TGC malformation and loss of trophoblast cells at the CP and EPC, were equivalent to *Cmas*$^{-/-}$ implants of untreated pregnant mice (Figure 4D). Also, the RM of *Cmas*$^{-/-}$ implants in neutrophil depleted mothers was still thickened and comparable to the RM of *Cmas*$^{-/-}$ implants of untreated mothers (Figure 4E). Taken together, these data demonstrate that the presence of maternal neutrophils was not causative for the observed embryonic and extraembryonic defects in *Cmas*$^{-/-}$ mice.

Maternal complement attack causes the *Cmas*$^{-/-}$ phenotype

Similar to humans, mice form a hemochorial type of placenta in which the maternal blood is in direct contact with fetal trophoblast cells (11). Hence, also humoral and complement components interact directly with fetal cells and their dysregulation is associated with pregnancy complications (35). To elucidate if activation of the maternal complement system is involved in the loss of fetal-maternal immune homeostasis in *Cmas*$^{-/-}$ pregnancies, we analysed the deposition of the central complement component 3 (C3) at E8.5. All implants, irrespective of their genotypes, revealed C3 staining at the interface between EPC and decidual stroma (Figure 5A). Apart from this, no C3 deposition was observed at the fetal-maternal border of control implants. In sharp contrast, C3 staining was observed along the entire fetal-maternal interface in *Cmas*$^{-/-}$ embryos. Especially TGCs exhibited strong C3 staining on their cell surface, suggesting an increased activation of the maternal complement system, whereas TGCs of control mice were devoid of C3 on the cell surface (Figure 5A, insets). In addition, control animals exhibited a prominent intracellular staining of C3 in the VE (Figure 5A, arrows), which was mostly absent in *Cmas*$^{-/-}$ implants. Differences in C3 deposition also occurred in mice that were depleted from maternal neutrophils, indicating that loss of neutrophils did not prevent complement activation on *Cmas*$^{-/-}$ TGCs (Figure 5B).
To evaluate whether the increased complement activation on fetal trophoblasts of *Cmas*$^{-/-}$ embryos evoked the phenotype of *Cmas*$^{-/-}$ implants, pregnant mice were injected with cobra venom factor (CVF) at E4.5 and E6.5. Along with serum proteins CVF forms a stable C3 convertase and exhausts C3 from the circulation. This technique has been successfully applied in various studies to decomplement mice (36). Depletion of C3 in CVF treated animals was verified by Western-blot analysis of sera isolated from PBS and CVF injected pregnant mice at E8.5 (Figure 6A). In *Cmas*$^{-/-}$ implants CVF injection reverted C3 deposition on TGCs (Figure 6B) and simultaneously reduced the number of maternal neutrophils at the fetal-maternal interface ($p < 0.001$) (Figure 6C and D). After CVF treatment C3 deposits as well as macrophage and neutrophil ($p > 0.05$) numbers were comparable in knockout and control implants (Figure S7).

Next, we analysed if C3 depletion also recues the defects observed in extraembryonic tissue of *Cmas*$^{-/-}$ embryos. Of note, as visualised by cytokeratin-8 staining, *Cmas*$^{-/-}$ implants of CVF treated females revealed a continuous layer of TGCs, as well as a restored EPC and CP indistinguishable from control implants in the same uterus (Figure 7A). To exclude the possibility that CVF treatment per se may alter embryonic or extraembryonic development, we carefully controlled wildtype implants isolated from CVF treated heterozygous dams with implants isolated from CVF treated and untreated wildtype dams. At histological level no sign of aberrant development induced by CVF could be identified.

The integrity of the CP in *Cmas*$^{-/-}$ embryos was addressed by analysing the expression of the CP marker CCAAT/enhancer binding protein-β (Cebpb), a transcription factor involved in placental vascularization (37,38). Cebpb was strongly expressed in the CP of control animals at E8.5 but almost absent in *Cmas*$^{-/-}$ CP (Figure 7A, PBS treated mice). Importantly, the Cebpb pattern in *Cmas*$^{-/-}$ implants was re-established upon CVF treatment, strongly suggesting that the CP was not only morphologically but also functionally restored (Figure 7A, CVF treated mice). CVF rescued *Cmas*$^{-/-}$ embryos maintained PNA reactivity on TGCs and other fetal trophoblast cells at the EPC, confirming their asialo nature equivalent to *Cmas*$^{-/-}$ embryos of untreated mothers (Figure 7A).

Beyond restoring trophoblast development, the maternal decomplementation also significantly decreased the thickness of the RM in *Cmas*$^{-/-}$ implants ($p < 0{,}001$) (Figure 7B and C), fully compensated the IUGR of *Cmas*$^{-/-}$ embryos ($p < 0{,}05$) (Figure 7D) and abrogated phenotypic variability of the embryo proper (Figure S8).

This experimental series clearly demonstrated that depletion of complement factor C3 by CVF treatment was sufficient to completely rescue the observed extraembryonic deficits as well as IUGR at E8.5 of *Cmas*$^{-/-}$ mice.

Loss of sialic acid activates the alternative complement pathway on the surface of TGCs

Activation of the complement cascade occurs through three major pathways, the classical, the lectin and the alternative pathway. To delineate which pathway is involved in the emergence of the *Cmas*$^{-/-}$ phenotype we analysed the presence of respective complement pathway marker proteins. The classical pathway is initiated by binding of antibodies to the cell surface and subsequent recognition of bound antibodies by C1q complexes. Neither control, nor *Cmas* negative trophoblasts were positive for C1q (Figure 8A). The classical and the lectin pathway both include cleavage of C4, making C4d a prevalently used marker for detection of classical and lectin pathway activation (39). C4d reactivity was observed in the maternal stroma adjacent to the EPC, but TGCs did not show any C4d staining in control or *Cmas*$^{-/-}$ implants (Figure 8B). The alternative complement pathway convertase C3bBb is stabilised by the fluid-phase component properdin (40). Similar to C3 deposition, properdin staining was absent on control trophoblasts, but very prominent on *Cmas*-negative TGCs, strongly indicating involvement of the alternative pathway (Figure 8C). Finally, we interrogated if complement activation results in formation of the membrane attack complex (MAC) and stained for the presence of the MAC component C9. However, no reactivity for C9 could be observed (Figure 8D).

DISCUSSION

Fetal development inside the womb has many benefits, a few of which are protection from fluctuations in nourishment, temperature and oxygen levels (41). Beyond the safety from external threats, fetal in utero existence however entails problems. Among the biggest challenges for mother and fetus is the establishment of immunologic coexistence of two genetically distinct entities, while simultaneously ensuring potent immune defense against pathogens. To date, several maternal and fetal mechanisms contributing to the establishment and maintenance of fetal-maternal immune homeostasis have been described (11). Yet, numerous non pathogen-related inflammatory reactions leading to pregnancy complications exist, which represent major threats to the developing fetus and its mother (42). Using a CMP-sialic acid negative mouse model, we demonstrated sialylation to be crucial for protection of fetal extraembryonic tissue from maternal complement attack, thereby guaranteeing its proper development which ultimately ensures adequate nourishment of the embryo proper.

The abundance of sialic acids and their outermost location on vertebrate cell surfaces enables sialoglycans to execute a myriad of functions, ranging from more global physicochemical functions to specific receptor-ligand mediated interactions (43). 15 years have passed since Horstkorte and colleagues showed genetic disruption of sialic acid de novo synthesis to cause embryonic lethality at E9.5 in mice (10). However, until today studies interrogating the underlying mechanisms are missing and little is known about the occurrence and functions of sialoglycans during embryonic development. MAA lectin analyses carried out in the current study revealed that α2,3-linked sialic acids were only sparsely found in the pre-streak embryo (E6.5), but were abundant on the cell surface of extraembryonic trophoblasts. This pattern was maintained for E8.5 implants with slight increase in the embryo proper (e.g. on ectodermal cells) and prominent staining in extraembryonic compartments, i.e. trophoblasts at the fetal-maternal interface. α2,3-linked sialic acids have also been described to be present on human trophoblasts facing the maternal blood or invading the maternal decidua, potentially indicating a similar function of α2,3-sialylation in different species with hemochorial placentation (44). Loss of CMAS in mice, however, was accompanied by a complete lack of MAA reactivity at all analysed time points. α2,6-linked sialic acids in control implants were prominent on embryonic ectoderm, amniotic and allantoic cells. Equivalent to α2,3-linked sialic acids, *Cmas*$^{-/-}$ embryos also revealed a lack of α2,6-sialylated glycans. Interestingly, control as well as *Cmas*$^{-/-}$ TGCs showed neuraminidase sensitive intracellular SNA staining. Since previous studies clearly demonstrated that loss of CMAS causes an asialo phenotype in embryonic stem cells in vitro and trophoblast cells are known to endocytose certain maternal proteins, e.g. immunoglobulins, the observed intracellular SNA reactivity in TGCs most likely represented internalised maternal material (9,45). Most notably, asialo *Cmas*$^{-/-}$ embryos established neuroepithelia, head mesenchyme as well as heart primordia and somites, promoting the hypothesis that sialoglycans are mostly dispensable for development of the embryo proper until E8.5. Although only few sialylated structures were detected with MAA in control embryos, this result was unexpected, also because the apical domain of the embryonic ectoderm showed unequivocal presence of α2,3-linked sialic acid already at E6.5. Moreover, previous reports postulated that sialylation of the apical domain of the embryonic ectoderm might contribute to the formation of the proamniotic cavity lumen by charge repulsion (46). Based on our current observation that all *Cmas*$^{-/-}$ mice have formed a proper proamniotic cavity by E6.5, the establishment of this lumen does apparently not exclusively rely on charge repulsion by sialoglycans but includes additional mechanisms.

Despite the large heterogeneity in embryonic development of E8.5 *Cmas*$^{-/-}$ epiblasts, all *Cmas*$^{-/-}$ implants featured a substantial IUGR, severe deficits in placental development and a thickened RM. The simultaneous extensive infiltration of maternal neutrophils into the fetal-maternal interface and increased deposition of C3 components favour the assumption that disturbance of the fetal-maternal immune homeostasis accounts for these phenotypic abnormalities. The decidua generates an immunologically privileged environment for the developing fetus by preventing the entry of certain types of leukocytes. B- and T-cells are prominent in the maternal blood but their numbers are drastically reduced in the pregnant decidua. Furthermore, decidual stromal cells are able to silence

the expression of chemokine genes needed for invasion of effector T-cells (22,23). As a consequence, the adaptive immune system is largely excluded from access to fetal tissue from early to mid-pregnancy. With some exceptions, this does not apply to the maternal innate immune system which is in direct contact with fetal trophoblasts at the EPC and TGCs.

It has been postulated that sialoglycans on the cell surface have evolved as an important mechanism of self-recognition, i.e. that Sia promotes discrimination between host tissue and pathogens (7). This immunomodulatory function is inter alia established through attenuation of immune responses by Siglecs, which are expressed by a wide range of adaptive and innate immune cells (5,47). Upon binding of the respective sialoglycan, some members of the Siglec family negatively regulate immune responses through their immune-receptor tyrosine-based inhibitory motifs (ITIM) (48;49). Murine neutrophils prominently express Siglec-E, which dampens the immune response of neutrophils upon binding to α2,3-linked sialylated glycans (50). The absence of Siglec-E ligands and the most probably abrogated Siglec-E mediated control of neutrophils in *Cmas*$^{-/-}$ trophoblasts implied that an excessive immune response by maternal neutrophils could account for the disturbed development of asialo trophoblasts. Even though neutrophil involvement in pregnancy complications in mice and humans is described (51), this hypothesis could be refuted since depletion of maternal neutrophils did not ameliorate any of the observed embryonic or extraembryonic deficits of *Cmas*$^{-/-}$ concepti. Taking into account that Siglec-E negatively influences immune responses of neutrophils also in group B *Streptococcus* and pulmonary inflammations (52), Siglec-E mediated self-recognition might not apply in the context of semi-allogeneic fetal trophoblasts in the absence of other proinflammatory stimuli.

CVF rescue experiments provided conclusive evidence that aberrant activation of the maternal complement pathway was a key cause of developmental deficits in *Cmas*$^{-/-}$ implants. Although CVF produces complement activation products, e.g. C3a and C5a in the serum of treated mice (53), neither *Cmas*$^{-/-}$ nor control littermates showed any adverse effect resulting from CVF injection. The CVF mediated depletion of C3 in the maternal serum abrogated excessive complement activation on asialo TGCs and at the same time restored development of the CP, EPC and TGCs. Strikingly, CVF treatment also prevented excessive thickening of the RM, restored growth of *Cmas*$^{-/-}$ embryos and prevented infiltration with maternal neutrophils. Considering that neutrophils are attracted by the complement cleavage products C3a and C5a, and that antibody induced depletion of neutrophils did not rescue the *Cmas*$^{-/-}$ phenotype, our data evidence that neutrophil recruitment to *Cmas*$^{-/-}$ implants was a secondary effect following excessive complement activation. This assumption probably also holds true for the slightly elevated numbers of decidual macrophages, since this effect was reverted by CVF injection and macrophages have been described to express anaphylotoxin receptors (54,55). Because extraembryonic tissues are crucial structures also in embryonic nourishment and waste exchange, we can conclude that deficits in their development most likely caused embryonic malnutrition and IUGR in *Cmas*$^{-/-}$ implants. Moreover, the proper development of extraembryonic tissues in *Cmas*$^{-/-}$ implants after CVF treatment argues for its independence from sialylation. In contrast, the establishment of the fetal-maternal immune homeostasis essentially depends on sialylation as demonstrated by the rescue of the *Cmas*$^{-/-}$ phenotype at E8.5 by complement depletion. Increased deposition of C3 on asialo TGCs was indicative for excessive complement activation, but did not allow discriminating between the potential pathways. C1q complexes are an essential part of classical complement pathway activation and C4d reactivity is an established diagnostic marker for activation of the classical and/or lectin complement pathway (39). Absence of both C1q and C4d strongly suggested that neither the classical nor the lectin pathway were involved in the pathogenesis of the *Cmas*$^{-/-}$ phenotype. Analysis of properdin, a potent stabiliser of the alternative pathway C3 convertase, however revealed increased reactivity on the cell surface of *Cmas*$^{-/-}$ TGCs (40). Taken together our data suggest that loss of sialylation on TGCs involved activation of the alternative complement pathway. However, increased levels of the membrane attack complex (MAC) monitored by C9 staining were not seen. Hence, developmental deficits observed in *Cmas*$^{-/-}$ extraembryonic tissues were by all likelihood not the result of cellular lysis, but were the consequences of other yet to be identified complement related mechanisms.

Similar to *Cmas*$^{-/-}$ implants, mice lacking the complement regulatory protein Crry exhibit a phenotype that includes excessive complement activation, neutrophil recruitment to the site of implantation, and deficits in placental development (56). It appears that failure or lack of one protective component, be it Sia or Crry, is sufficient to unhinge regulation of the complement system, underpinning the fragility of complement regulation at the fetal-maternal interface. The fact that human trophoblasts express numerous complement regulating proteins, further highlights the importance of a well-orchestrated protection against the maternal complement system in hemochorial placentation (20). Also noteworthy is the deposition of C3 at the EPC that was observed in all analysed genotypes and has previously been reported (56). This supports the speculation that controlled complement activation may be physiological in placental development, e.g. to stimulate remodelling of the fetal-maternal interface at the EPC and clearance of cellular debris.

The mechanisms that induce activation of the alternative complement pathway in *Cmas*$^{-/-}$ mice remain unclear. One possible explanation might be an impaired function of factor H (CFH), a serum protein and negative regulator of the complement cascade. Upon binding CFH destabilises existing C3 convertases and recruits factor I, which cleaves C3b and thus prevents C3 convertase complex formation (57). Recently, Blaum and coworkers demonstrated that efficient recruitment of CFH to the cell surface requires the presence of α2,3-sialylated glycans (5). Furthermore, mutations in the *CFH* gene affecting the sialic acid recognition site have been associated with the atypical haemolytic syndrome, a pathology characterised by excessive activation of the complement system (5,58). However, CFH deficient mice are fertile and the complement system is intricately regulated by a multitude of factors (59). Thus, the mechanisms that disequilibrated the complement system in *Cmas*$^{-/-}$ embryos could not yet be addressed in our mouse model and require further investigations. Our future work will make use of conditional *Cmas* mice allowing the depletion of CMAS in a cell type specific manner (e.g. individual trophoblast cell types or embryo proper) and by crossing in the C3 knockout.

Finally it is worth mentioning that preeclampsia, a pregnancy complication that affects 2-8% of all pregnancies, involves excessive activation of the complement system and decidual inflammatory reactions, leading to placental deficits, IUGR and maternal cardiovascular complications (60,61). To date, the mechanisms causing inflammation remain unclear and medical intervention is limited to the treatment of symptoms. Interestingly, Sia related genes, such as the sialyltransferase ST6Gal1, Siglec-6 and sialic acid acetylesterase (SIAE) are reported to be differentially regulated in placentae of preeclamptic women, providing a first clue that aberrant sialylation might be involved in this pathology (62,63). Further studies are needed to fully evaluate the molecular details by which sialylation might be involved in the pathogenesis of pregnancy complications and if the absence of specific sialoglycans could serve as a potential diagnostic marker.

In conclusion, the constitutive *Cmas* mouse model presented here and its available conditional variants are valuable tools to specifically investigate the impact of sialylation on the regulation of the complement system, not only during pregnancy but also in immunologically challenging situations, e.g. after organ transplantations.

METHODS

Mice

To inactivate the *Cmas* gene, exon 4 encoding for the active site of the protein was deleted using the frt/loxP system as described (9). The neomycin-cassette was deleted by crossing $Cmas^{neo}$ homozygous mice with the Flp-deleter strain *SJL-Tg(ACTFLPe)9205Dym/J*. Resulting $Cmas^{floxed}$ mice were bred to homozygosity and crossed with the Cre-deleter strain *C57BL/6-Tg(Zp3-cre)93Knw/J*. Upon six backcrosses with NMRI mice heterozygous *Cmas* knockout mice ($Cmas^{+/-}$) were obtained. Intercrosses of 3-6 month old $Cmas^{+/-}$ animals gave rise to $Cmas^{-/-}$, $Cmas^{+/-}$ and $Cmas^{+/+}$ embryos, the latter two referred to as controls. Genotyping was done by PCR as depicted in Figure S1A, B. The following primers were used: BWF59 (5`AGCGCCTGTGTACCCCTCTTA3`), BWB58 (5`GCGAGCAGCAAGTGAGCA3`) and AMB40 (5`TCAAGTTCAGAGGCTCAGTCACTTCACG3`); the PCR program included three steps (98°C 30sec, 66°C 30sec, 72°C 30sec) and 30 cycles. Animals were obtained from and hosted in the animal facility of the Hannover Medical School under specific pathogen-free conditions. All animal experiments were carried out in compliance with German law for protection of animals and were approved by the local authorities (TV 33.12–42502-04-16/2346).

Histology and quantification of IUGR

Female mice of heterozygous $Cmas^{+/-}$ matings were checked daily in the early morning for vaginal plug. The time point of plug discovery was considered as day 0.5 after conception. On day 6.5, 7.5 and 8.5 of gestation, pregnant mice were sacrificed, and the uteri were dissected and fixed in 4% paraformaldehyde in PBS o/n at 4°C. After fixation, the uteri were dehydrated in a graded ethanol series and embedded in paraffin. For histological analyses, paraffin embedded uteri were sectioned in 3 µm slices using a microtome, rehydrated and stained with hematoxlyin and eosin. Slices were analysed by a Zeiss ObserverZ1 microscope equipped with a Zeiss AxioCam MRc camera. To quantify intrauterine growth restriction, the sum of the areas of amniotic cavity, exocoelomic cavity, ectoplacental cavity and embryo proper as depicted in Figure S3 were measured using Zeiss ZEN software. Statistical analyses were performed in GraphPad Prism software where $P < 0.05$ was considered significant.

Lectin assays on uterus sections

For detection of α2,3-linked sialic acid rehydrated tissue slices were probed with *Maackia amurensis* agglutinin, 1:800 (MAA, DIG Glycan Differentiation Kit, Roche) at 4°C o/n with subsequent incubation with peroxidase coupled anti-DIG Fab fragments, 1:1000 (Roche). Signals were enhanced by biotin tyramide, 2,5 µg/ml (Iris Biotech) amplification for 10 minutes at room temperature and detected by Strepavidin-Cy3, 1:2000 (Rockland). For detection of α2,6-linked sialic acid rehydrated tissue slices were probed with biotinylated *Sambucus nigra* agglutinin, 1:250 (SNA, Vector) at 4°C o/n with subsequent detection by Strepavidin-Cy3, 1:500 (Rockland). Control slides were treated with *Arthrobacter ureafaciens* neuraminidase (EY Laboratories) at room temperature o/n prior to MAA incubation. For simultaneous detection of free galactose residues, Alexa Fluor® 647 conjugated *Arachis hypogaea* agglutinin (PNA, Sigma-Aldrich) was added during incubation with Strepavidin-Cy3. Decidual NK cells were detected by biotinylated *Dolichos biflorus* agglutinin (DBA), 1:2000 (Vector) and subsequently stained with strepavidin-HRP, 1:500 (Vector). DBA positive cells were detected by 3,3'-Diaminobenzidine (DAB, Dako) reaction, subsequently counterstained with hematoxylin and analysed in the aforementioned microscope setup.

Immunohistochemistry and indirect immunofluorescence analyses

Tissues were paraffin fixed and embedded according to H&E staining. For immunohistochemistry (IHC) and immunofluorescence analyses, antigen retrieval (Dako) was performed after rehydration. Slices were then blocked with 1% BSA in PBS and incubated with the respective antibody in blocking solution. The following dilutions for primary antibodies were applied: Cytokeratin-8, 1:20.00 (TROMA-I, DSHB, AB 531826); Collagen-IV, 1:200 (Millipore, AB756P); Laminin, 1:30 (Sigma, L9393); Gr-1, 1:50 (BD Biosciences, RB6-8C5); F4/80, 1:50 (AbD Serotec, CI:A3-1); anti-Ly6G, 1:100.000 (BioXCell, 1A8) ; C3, 1:20.000 (Cappel, MP Biomedicals, 55463); C1q 1:50

(Biorbyt, orb155963), C4d 1:50 (Hycult Biotech, HP8033); Properdin 1:2000 (Complement Technologies, A139); C9 1:10.000 (Paul B. Morgan, University Hospital of Wales, Cardiff University, Heath Park, Cardiff, CF14 4XN, UK), Cebpb, 1:20 (Santa Cruz, H-7). Cebpb antibody was pre-incubated with biotinylated anti-mouse IgG Fab fragments prior to use (ARK kit, Dako, K3954) according to the manufacturer's guidelines. Secondary antibodies: anti-rabbit IgG-Cy3, 1:500 (Sigma, C2306); anti-rabbit IgG- 1:500 (Sigma, A0545); anti-goat IgG, 1:500 (Santa Cruz, SC-2020). Biotinylation was detected using strepavidin-HRP, 1:500 (Dako, P0397) and the signal was amplified by biotin tyramide, 2,5 µg/ml (Iris Biotech) treatment for 10 minutes at room temperature. Strepavidin-Cy3, 1:500 (Rockland, S000-04) served as detection system). For detection of Gr-1 a biotinylated anti-rat antibody (1:500, Boehringer, 1348779) was used, followed by strepavidin-HRP, 1:500 (Dako, P0397). Cytokeratin-8 and Ly6G were detected using the ImmPRESS™ HRP anti-rat IgG (Vector, MP-7444) conjugate. All HRP-conjugated reagents were detected by 3,3'-Diaminobenzidine (DAB) reaction, subsequently counterstained with hematoxylin and analysed in the aforementioned microscope setup.

In situ hybridisation experiments

In situ hybridizations were performed on 10 µm sections. Riboprobes were synthesised by T3 or T7 polymerases using DIG-labelled UTP (Roche). Specific hybridisation was detected by incubation with anti-DIG alkaline phosphatase (Roche) and subsequent staining with BCIP/NBT.

Quantification of decidual leukocyte populations

Identification of leukocytes was accomplished by IHC of described marker proteins, i.e. Gr-1/Ly6G (neutrophils), DBA (decidual NK cells) or F4/80 (macrophages). Gr-1/Ly6G positive cells located in the maternal decidua were counted, whereby positive cells in the maternal vasculature were excluded. Also F4/80 positive cells were quantified in the entire maternal decidua. DBA positive cells were quantified in the decidua basalis. In all of the mentioned leukocyte quantifications, also the total area of the decidua was measured and the ratio of positive leukocytes per mm² (for Gr-1, Ly6G and F4/80) or $\mu m^2/10^5$ (for DBA) was calculated. For comparing decidual leukocytes of control versus *Cmas*$^{-/-}$ implants a Student's t-test was applied.

Depletion of neutrophils from maternal blood

Heterozygous *Cmas*$^{+/-}$ mice were mated as described and 500 µg anti-Ly6G (1A8, BioXCell) or isotype control antibody (2A3, BioXCell) diluted in 100 µl PBS were intraperitoneally injected into pregnant mice at day E4.5. The uteri of Ly6G treated mice were removed at E8.5 and the uterus of the isotype control treated mouse was removed at E9.5. To verify the successful depletion of maternal neutrophils, blood from Ly6G or from untreated mice was analysed by FACS in a FACScalibur machine (Beckton & Dickinson) and raw data were analysed using FlowJo (TreeStar). Blood was obtained from the abdominal aorta with a heparinised syringe after cervical dislocation and treated with red blood cell lysis buffer for 10 minutes at room temperature. For the FACS analyses 0,2 mg/ml anti-Ly6G (1A8, BioXCell) or 0,2 mg/ml isotype control rat IgG2a (2A3, BioXCell) was used as primary antibody and anti-rat IgG-Cy3, 1:200 (AP189C, EMD Millipore) as secondary antibody. Cells were gated for lymphocytes, monocytes and granulocytes using the forward scatter, before subsequent analysis of Ly6G positive cells.

Decomplementation of pregnant mice

Three individual pregnant *Cmas*$^{+/-}$ mice were intraperitoneally injected at E4.5 and E6.5 two times at these days at 10 am and 2 pm with either 5 U of cobra venom factor (CVF) (Quidel) in 100 µl PBS or PBS only for each injection. They were killed at day 8.5 of pregnancy and *Cmas*$^{-/-}$ and control littermates were analysed. Depletion of C3 in the serum of CVF treated animals was confirmed by western blot: 0.25 µl serum was separated by 12% SDS-PAGE under reducing conditions, transferred to PVDF membrane and incubated with the primary antibodies goat anti-C3, 1:5.000 (Cappel, MP Biomedicals) or goat anti-albumin, 1:5.000 (ab19194, Abcam) for loading control. After

incubation with anti-goat HRP-conjugated secondary antibody, 1:15.000 (sc-2020, Santa Cruz) detection was performed with enhanced chemoluminescence.

Statistics

Comparisons of fetal size (Figure 2B, Figure 4C), Gr-1 positive cells (Figure 3A), DBA positive cells (Figure 3A) and F4/80 positive cells (Figure 3A, Figure S7) were analysed by two-tailed unpaired *t* test. Statistical analysis of quantifications of Ly6G positive cells (Figure 6A), fetal size (Figure 6D) and Reichert's membrane thickness (Figure 6C) after treatment with CVF or PBS were analysed by one-way ANOVA, followed by Newman-Keuls post-test. All analyses were performed using GraphPad Prism software and $P < 0,05$ was considered significant.

Study approval

All animal experiments were approved by the "Niedersaechsisches Landesamt fuer Verbraucherschutz und Lebensmittelsicherheit (LAVES)", Postfach 3949, 26029 Oldenburg, Germany, AZ 33.12-42502-04-16/2346 and from the „Institut fuer Versuchstierkunde und Zentrales Tierlaboratorium", Hannover Medical School, Carl-Neuberg-Str. 1, 30625 Hannover, Germany, Head Prof. André Bleich.

509 **Author contributions**

510 Conceptualisation, R.G.S., A.M.K. and B.W.; Methodology, M.A., A.M.K., A.K., S.T. and B.W.; Validation, M.A. and
511 B.W.; Formal analysis, M.A. and B.W.; Investigation, M.A., I.A., K.F.S. and U.B.P.; Generation of *Cmas* mutant mice,
512 B.W.; Resources, A.K., R.G.S., S.T., A.M.K. and B.W.; Writing-Original Draft, M.A., A.M.K. and B.W.; Visualisation,
513 M.A. and B.W.; Supervision, R.G.S., A.M.K. and B.W., Funding Acquisition, R.G.S., A.M.K. and B.W.

514

Acknowledgements

We thank Mania Ackermann for help with the FACS analyses, Carina Weiss for support regarding in situ hybridisations and Adrian Erlebacher and Susan Fisher for critical and helpful discussion of the data. Also we would like to thank Paul B. Morgan (Cardiff University) for kindly providing anti-C9 antibody. Anja Münster-Kühnel and Birgit Weinhold were supported by grants from the Deutsche Forschungsgemeinschaft (DFG, MU 1849/2-1 and WE 5585/1-1).

References

1. Moremen KW, Tiemeyer M, Nairn AV. Vertebrate protein glycosylation: diversity, synthesis and function. *Nat Rev Mol Cell Biol*. 2012;13(7):448-462.

2. Fujitani N, Furukawa J, Araki K, Fujioka T, Takegawa Y, Piao J, Nishioka T, Tamura T, Nikaido T, Ito M *et al*. Total cellular glycomics allows characterizing cells and streamlining the discovery process for cellular biomarkers. *Proc Natl Acad Sci U S A*. 2013;110(6):2105-2110.

3. Cohen M, Varki A. The sialome--far more than the sum of its parts. *OMICS*. 2010;14(4):455-464.

4. Bhide GP, Colley KJ. Sialylation of N-glycans: mechanism, cellular compartmentalization and function. *Histochem Cell Biol*. 2017;147(2):149-174.

5. Blaum BS, Hannan JP, Herbert AP, Kavanagh D, Uhrin D, Stehle T. Structural basis for sialic acid-mediated self-recognition by complement factor H. *Nat Chem Biol*. 2015;11(1):77-82.

6. Crocker PR, Paulson JC, Varki A. Siglecs and their roles in the immune system. *Nat Rev Immunol*. 2007;7(4):255-266.

7. Varki A, Gagneux P. Multifarious roles of sialic acids in immunity. *Ann N Y Acad Sci*. 2012;125316-36.

8. Kean EL, Münster-Kühnel AK, Gerardy-Schahn R. CMP-sialic acid synthetase of the nucleus. *Biochim Biophys Acta*. 2004;1673(1-2):56-65.

9. Abeln M, Borst KM, Cajic S, Thiesler H, Kats E, Albers I, Kuhn M, Kaever V, Rapp E, Münster-Kühnel A *et al*. Sialylation Is Dispensable for Early Murine Embryonic Development in Vitro. *Chembiochem*. 2017;18(13):1305-1316.

10. Schwarzkopf M, Knobeloch KP, Rohde E, Hinderlich S, Wiechens N, Lucka L, Horak I, Reutter W, Horstkorte R. Sialylation is essential for early development in mice. *Proc Natl Acad Sci U S A*. 2002;99(8):5267-5270.

11. Prabhudas M, Bonney E, Caron K, Dey S, Erlebacher A, Fazleabas A, Fisher S, Golos T, Matzuk M, McCune JM *et al*. Immune mechanisms at the maternal-fetal interface: perspectives and challenges. *Nat Immunol*. 2015;16(4):328-334.

12. Marikawa Y, Alarcon VB. Establishment of trophectoderm and inner cell mass lineages in the mouse embryo. *Mol Reprod Dev*. 2009;76(11):1019-1032.

13. Bielinska M, Narita N, Wilson DB. Distinct roles for visceral endoderm during embryonic mouse development. *Int J Dev Biol*. 1999;43(3):183-205.

14. Schrode N, Xenopoulos P, Piliszek A, Frankenberg S, Plusa B, Hadjantonakis AK. Anatomy of a blastocyst: cell behaviors driving cell fate choice and morphogenesis in the early mouse embryo. *Genesis*. 2013;51(4):219-233.

15. Watson ED, Cross JC. Development of structures and transport functions in the mouse placenta. *Physiology (Bethesda)*. 2005;20180-193.

16. Rai A, Cross JC. Development of the hemochorial maternal vascular spaces in the placenta through endothelial and vasculogenic mimicry. *Dev Biol*. 2014;387(2):131-141.

17. Apps R, Murphy SP, Fernando R, Gardner L, Ahad T, Moffett A. Human leucocyte antigen (HLA) expression of primary trophoblast cells and placental cell lines, determined using single antigen beads to characterize allotype specificities of anti-HLA antibodies. *Immunology*. 2009;127(1):26-39.

18. Hunt JS, Fishback JL, Andrews GK, Wood GW. Expression of class I HLA genes by trophoblast cells. Analysis by in situ hybridization. *J Immunol*. 1988;140(4):1293-1299.

19. Madeja Z, Yadi H, Apps R, Boulenouar S, Roper SJ, Gardner L, Moffett A, Colucci F, Hemberger M. Paternal MHC expression on mouse trophoblast affects uterine vascularization and fetal growth. *Proc Natl Acad Sci U S A*. 2011;108(10):4012-4017.

20. Holmes CH, Simpson KL, Okada H, Okada N, Wainwright SD, Purcell DF, Houlihan JM. Complement regulatory proteins at the feto-maternal interface during human placental development: distribution of CD59 by comparison with membrane cofactor protein (CD46) and decay accelerating factor (CD55). *Eur J Immunol*. 1992;22(6):1579-1585.

21. Xu C, Mao D, Holers VM, Palanca B, Cheng AM, Molina H. A critical role for murine complement regulator crry in fetomaternal tolerance. *Science*. 2000;287(5452):498-501.

22. Nancy P, Tagliani E, Tay CS, Asp P, Levy DE, Erlebacher A. Chemokine gene silencing in decidual stromal cells limits T cell access to the maternal-fetal interface. *Science*. 2012;336(6086):1317-1321.

23. Zhao H, Kalish F, Schulz S, Yang Y, Wong RJ, Stevenson DK. Unique roles of infiltrating myeloid cells in the murine uterus during early to midpregnancy. *J Immunol*. 2015;194(8):3713-3722.

24. Girardi G, Berman J, Redecha P, Spruce L, Thurman JM, Kraus D, Hollmann TJ, Casali P, Caroll MC, Wetsel RA *et al*. Complement C5a receptors and neutrophils mediate fetal injury in the antiphospholipid syndrome. *J Clin Invest*. 2003;112(11):1644-1654.

25. Jeyabalan A. Epidemiology of preeclampsia: impact of obesity. *Nutr Rev*. 2013;71 Suppl 1S18-S25.

26. Srinivas SK, Edlow AG, Neff PM, Sammel MD, Andrela CM, Elovitz MA. Rethinking IUGR in preeclampsia: dependent or independent of maternal hypertension? *J Perinatol*. 2009;29(10):680-684.

27. Novogrodsky A, Lotan R, Ravid A, Sharon N. Peanut agglutinin, a new mitogen that binds to galactosyl sites exposed after neuraminidase treatment. *J Immunol*. 1975;115(5):1243-1248.

28. Simmons DG, Cross JC. Determinants of trophoblast lineage and cell subtype specification in the mouse placenta. *Dev Biol*. 2005;284(1):12-24.

29. Tamai Y, Ishikawa T, Bosl MR, Mori M, Nozaki M, Baribault H, Oshima RG, Taketo MM. Cytokeratins 8 and 19 in the mouse placental development. *J Cell Biol*. 2000;151(3):563-572.

30. Jollie WP. Changes in the fine structure of the parietal yolk sac of the rat placenta with increasing gestational age. *Am J Anat*. 1968;122(3):513-531.

31. Sheng G, Foley AC. Diversification and conservation of the extraembryonic tissues in mediating nutrient uptake during amniote development. *Ann N Y Acad Sci*. 2012;127197-103.

32. Croy BA, Chantakru S, Esadeg S, Ashkar AA, Wei Q. Decidual natural killer cells: key regulators of placental development (a review). *J Reprod Immunol*. 2002;57(1-2):151-168.

33. Zhang JH, Yamada AT, Croy BA. DBA-lectin reactivity defines natural killer cells that have homed to mouse decidua. *Placenta*. 2009;30(11):968-973.

34. Daley JM, Thomay AA, Connolly MD, Reichner JS, Albina JE. Use of Ly6G-specific monoclonal antibody to deplete neutrophils in mice. *J Leukoc Biol*. 2008;83(1):64-70.

35. Lynch AM, Salmon JE. Dysregulated complement activation as a common pathway of injury in preeclampsia and other pregnancy complications. *Placenta*. 2010;31(7):561-567.

36. van den Berg CW, Aerts PC, Van Dijk H. In vivo anti-complementary activities of the cobra venom factors from Naja naja and Naja haje. *J Immunol Methods*. 1991;136(2):287-294.

37. Begay V, Smink J, Leutz A. Essential requirement of CCAAT/enhancer binding proteins in embryogenesis. *Mol Cell Biol*. 2004;24(22):9744-9751.

38. Simmons DG, Natale DR, Begay V, Hughes M, Leutz A, Cross JC. Early patterning of the chorion leads to the trilaminar trophoblast cell structure in the placental labyrinth. *Development*. 2008;135(12):2083-2091.

39. Murata K, Baldwin WM, III. Mechanisms of complement activation, C4d deposition, and their contribution to the pathogenesis of antibody-mediated rejection. *Transplant Rev (Orlando)*. 2009;23(3):139-150.

40. Hourcade DE. The role of properdin in the assembly of the alternative pathway C3 convertases of complement. *J Biol Chem*. 2006;281(4):2128-2132.

41. Maltepe E, Fisher SJ. Placenta: the forgotten organ. *Annu Rev Cell Dev Biol*. 2015;31523-552.

42. Nadeau-Vallee M, Obari D, Palacios J, Brien ME, Duval C, Chemtob S, Girard S. Sterile inflammation and pregnancy complications: a review. *Reproduction*. 2016;152(6):R277-R292.

43. Varki A. Glycan-based interactions involving vertebrate sialic-acid-recognizing proteins. *Nature*. 2007;446(7139):1023-1029.

44. Chen Q, Pang PC, Cohen ME, Longtine MS, Schust DJ, Haslam SM, Blois SM, Dell A, Clark GF. Evidence for Differential Glycosylation of Trophoblast Cell Types. *Mol Cell Proteomics*. 2016;15(6):1857-1866.

45. Bevilacqua E, Hoshida MS, Amarante-Paffaro A, Albieri-Borges A, Zago GS. Trophoblast phagocytic program: roles in different placental systems. *Int J Dev Biol*. 2010;54(2-3):495-505.

46. Bedzhov I, Graham SJ, Leung CY, Zernicka-Goetz M. Developmental plasticity, cell fate specification and morphogenesis in the early mouse embryo. *Philos Trans R Soc Lond B Biol Sci*. 2014;369(1657).

47. Macauley MS, Crocker PR, Paulson JC. Siglec-mediated regulation of immune cell function in disease. *Nat Rev Immunol*. 2014;14(10):653-666.

48. Lock K, Zhang J, Lu J, Lee SH, Crocker PR. Expression of CD33-related siglecs on human mononuclear phagocytes, monocyte-derived dendritic cells and plasmacytoid dendritic cells. *Immunobiology*. 2004;209(1-2):199-207.

49. McMillan SJ, Sharma RS, McKenzie EJ, Richards HE, Zhang J, Prescott A, Crocker PR. Siglec-E is a negative regulator of acute pulmonary neutrophil inflammation and suppresses CD11b beta2-integrin-dependent signaling. *Blood*. 2013;121(11):2084-2094.

50. Chang YC, Olson J, Beasley FC, Tung C, Zhang J, Crocker PR, Varki A, Nizet V. Group B Streptococcus engages an inhibitory Siglec through sialic acid mimicry to blunt innate immune and inflammatory responses in vivo. *PLoS Pathog*. 2014;10(1):e1003846.

51. Giaglis S, Stoikou M, Grimolizzi F, Subramanian BY, van Breda SV, Hoesli I, Lapaire O, Hasler P, Than NG, Hahn S. Neutrophil migration into the placenta: Good, bad or deadly? *Cell Adh Migr*. 2016;10(1-2):208-225.

52. McMillan SJ, Sharma RS, Richards HE, Hegde V, Crocker PR. Siglec-E promotes beta2-integrin-dependent NADPH oxidase activation to suppress neutrophil recruitment to the lung. *J Biol Chem*. 2014;289(29):20370-20376.

53. Goldman JN, Bangalore S, Goldman MB. Activation of murine complement by cobra venom factor in the presence of EDTA. *J Immunol*. 1979;123(5):2421-2427.

54. Chenoweth DE, Goodman MG, Weigle WO. Demonstration of a specific receptor for human C5a anaphylatoxin on murine macrophages. *J Exp Med*. 1982;156(1):68-78.

55. Quell KM, Karsten CM, Kordowski A, Almeida LN, Briukhovetska D, Wiese AV, Sun J, Ender F, Antoniou K, Schroder T *et al*. Monitoring C3aR Expression Using a Floxed tdTomato-C3aR Reporter Knock-in Mouse. *J Immunol*. 2017;199(2):688-706.

56. Mao D, Wu X, Deppong C, Friend LD, Dolecki G, Nelson DM, Molina H. Negligible role of antibodies and C5 in pregnancy loss associated exclusively with C3-dependent mechanisms through complement alternative pathway. *Immunity*. 2003;19(6):813-822.

57. Ferreira VP, Pangburn MK, Cortes C. Complement control protein factor H: the good, the bad, and the inadequate. *Mol Immunol*. 2010;47(13):2187-2197.

58. Hyvarinen S, Meri S, Jokiranta TS. Disturbed sialic acid recognition on endothelial cells and platelets in complement attack causes atypical hemolytic uremic syndrome. *Blood*. 2016;127(22):2701-2710.

59. Ricklin D, Reis ES, Lambris JD. Complement in disease: a defence system turning offensive. *Nat Rev Nephrol*. 2016;12(7):383-401.

60. Sibai B, Dekker G, Kupferminc M. Pre-eclampsia. *Lancet*. 2005;365(9461):785-799.

61. Wang W, Irani RA, Zhang Y, Ramin SM, Blackwell SC, Tao L, Kellems RE, Xia Y. Autoantibody-mediated complement C3a receptor activation contributes to the pathogenesis of preeclampsia. *Hypertension*. 2012;60(3):712-721.

62. Tsai S, Hardison NE, James AH, Motsinger-Reif AA, Bischoff SR, Thames BH, Piedrahita JA. Transcriptional profiling of human placentas from pregnancies complicated by preeclampsia reveals disregulation of sialic acid acetylesterase and immune signalling pathways. *Placenta*. 2011;32(2):175-182.

63. Winn VD, Gormley M, Paquet AC, Kjaer-Sorensen K, Kramer A, Rumer KK, Haimov-Kochman R, Yeh RF, Overgaard MT, Varki A *et al*. Severe preeclampsia-related changes in gene expression at the maternal-fetal interface include sialic acid-binding immunoglobulin-like lectin-6 and pappalysin-2. *Endocrinology*. 2009;150(1):452-462.

Figure 1. *Cmas*$^{-/-}$ embryos lack sialylation. (A) Lectin binding epitopes for *Maackia amurensis* agglutinin (MAA) detecting terminal α2,3 linked sialic acid and for peanut agglutinin (PNA) detecting terminal galactose. **(B)** Sagittal paraffin sections of uteri with E6.5 and E8.5 implants were co-stained with the lectins MAA (red) and PNA (green). Insets show trophoblast giant cells lining the fetal-maternal interface. The area of the ectoplacental cone (EPC) is indicated by brackets. MAA positive cells in *Cmas*$^{-/-}$ (inset, magnified) are maternal leukocytes. Asterisks indicate Reichert's membrane; arrows mark the apical side of ectodermal epithelia and arrowheads indicate mesenchymal cells. MAA specificity was confirmed by neuraminidase treatment of sagittal paraffin sections prior to lectin staining. Neuraminidase releases sialic acid from glycans and thereby depletes MAA binding epitopes. Simultaneously, removal of Sia exposes underlying galactose to PNA binding. Scale bar in the insets: 50 µm. Nuclei were stained with DAPI and are shown in white. Representative images from n=3 (E6.5 control and *Cmas*$^{-/-}$, E8.5 *Cmas*$^{-/-}$) and n=5 (E8.5 control) embryos within uterus.

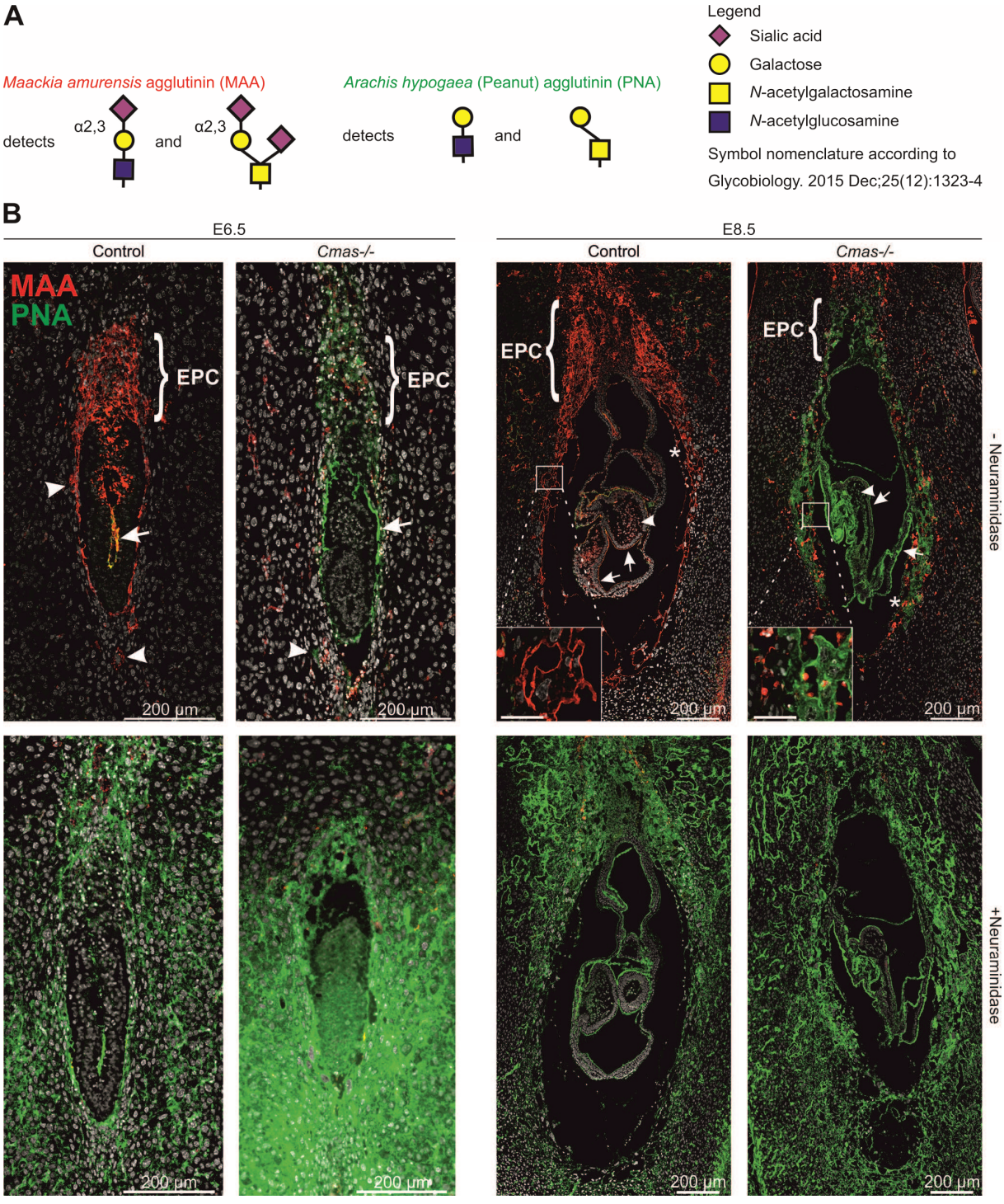

Figure 2. *Cmas*$^{-/-}$ mice exhibit intrauterine growth restriction and extraembryonic developmental deficits. (A) Hematoxylin and eosin stained sagittal paraffin sections of uteri at E6.5, E7.5 and E8.5. Insets show mesenchymal mesoderm cells migrating from posterior to anterior. Proamniotic cavity (PC); visceral endoderm (VE); embryonic ectoderm (EC); mesoderm (ME); heart (H); somite (S). Scale bars in the insets: 12,5 µm. Representative images of at least 3 embryos within the uterus for each genotype and time point. **(B)** Mean fetal size as measured by the sum of the areas of amniotic cavity, exocoelomic cavity, ectoplacental cavity and embryo proper in (µm²/10^5), for schematic overview of measured areas see Figure S5. E6.5 (control n=4, *Cmas*$^{-/-}$ n=5), E7.5 (control n=4, *Cmas*$^{-/-}$ n=4), E8.5 (control n=6, *Cmas*$^{-/-}$ n=7). Error bars indicate SD. Statistical analyses were performed by Student's t-test. (*P < 0.05). **(C)** Immunohistochemical detection of Cytokeratin-8 as marker for trophoblast cells on sagittal paraffin sections of E8.5 uteri. Trophoblast giant cells (TGC) and the chorionic plate (CP) are indicated by arrows, internal trophoblasts of the EPC by arrowheads. The border of the ectoplacental cone (EPC) is marked by dotted lines. Representative images of n=3 embryos for each genotype. **(D)** Collagen IV and Laminin indirect immunofluorescence staining on sagittal paraffin sections of uteri at E8.5 to visualise Reichert's membrane (arrow) and parietal endoderm (arrowheads). Nuclei stained with DAPI are shown in white. Representative images of n=3 embryos for each genotype.

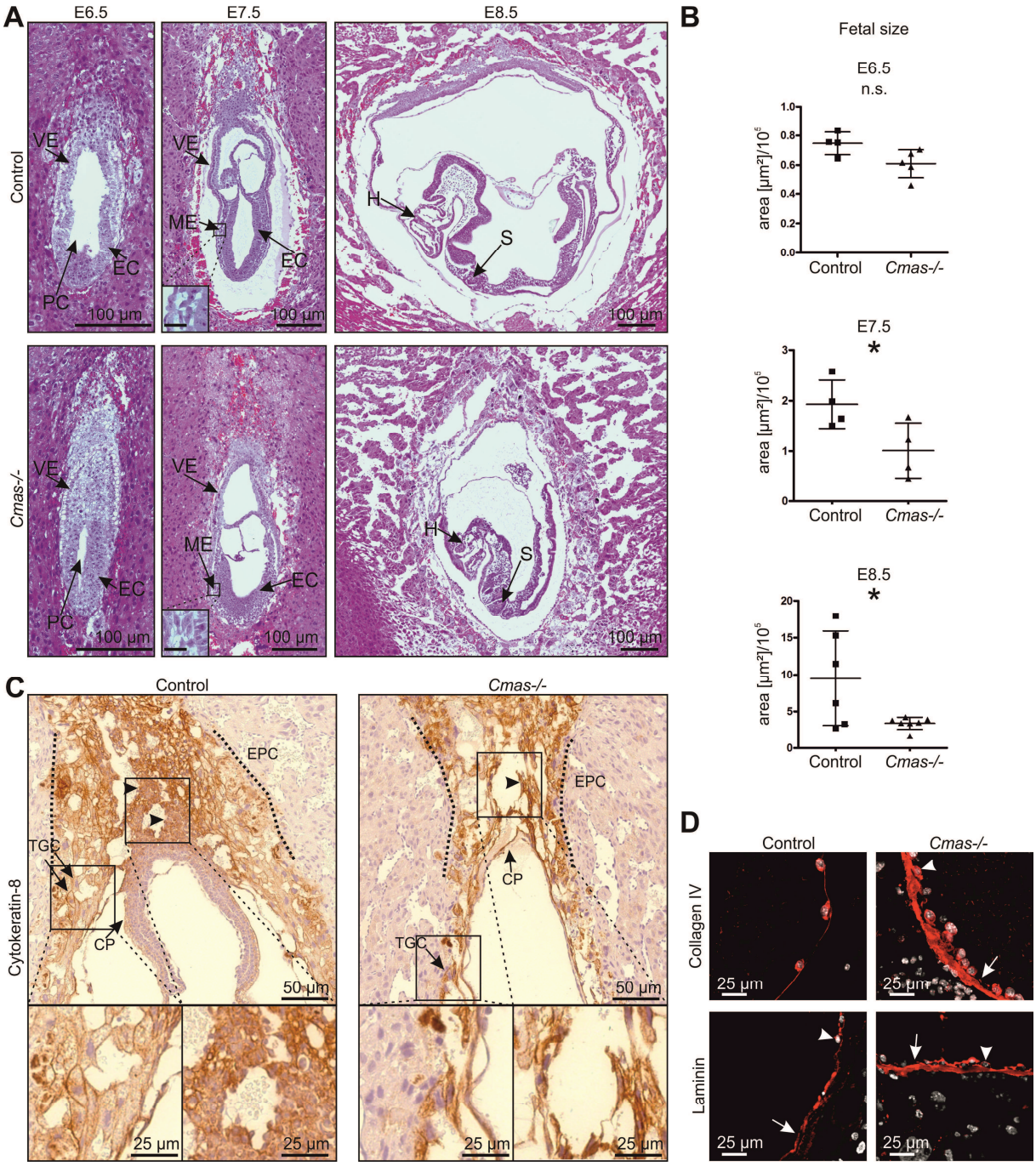

Figure 3. Infiltration of the fetal-maternal interface of *Cmas*$^{-/-}$ animals by maternal neutrophils. (A) Gr-1 (neutrophils) immunohistochemical staining and quantification of Gr-1-positive cells surrounding fetal tissues of sagittal paraffin sections of uteri at E6.5 to E8.5. Insets show Gr-1 positive cells at the ectoplacental cone and in the vicinity of fetal trophoblasts at the antimesometrial pole. E6.5 (control n=4, *Cmas*$^{-/-}$ n=5), E7.5 (control n=4, *Cmas*$^{-/-}$ n=4) and E8.5 (control n=5, *Cmas*$^{-/-}$ n=5). Error bars indicate SD. Scale bars in the insets: 12,5 µm. **(B)** DBA lectin (decidual NK cells) immunohistochemical staining and quantification of sagittal paraffin sections of uteri at E6.5 to E8.5. Mean number of DBA lectin positive cells in the decidua basalis. E6.5 (control n=4, *Cmas*$^{-/-}$ n=5), E7.5 (control n=8, *Cmas*$^{-/-}$ n=5), E8.5 (control n=5, *Cmas*$^{-/-}$ n=3). Error bars indicate SD. Staining of visceral endoderm was only observed in control implants. **(C)** F4/80 (macrophages) immunohistochemical staining and quantification of sagittal paraffin sections of uteri from E6.5 to E8.5. Statistical analysis of the number of F4/80 postive cells surrounding fetal tissues. E6.5 (control n=4, *Cmas*$^{-/-}$ n=4), E7.5 (control n=6, *Cmas*$^{-/-}$ n=5), E8.5 (control n=4, *Cmas*$^{-/-}$ n=5). Scale bars in the insets: 25 µm. Error bars indicate SD. All statistical analyses were performed by Student's t-test **P < 0.01; ***P < 0.001).

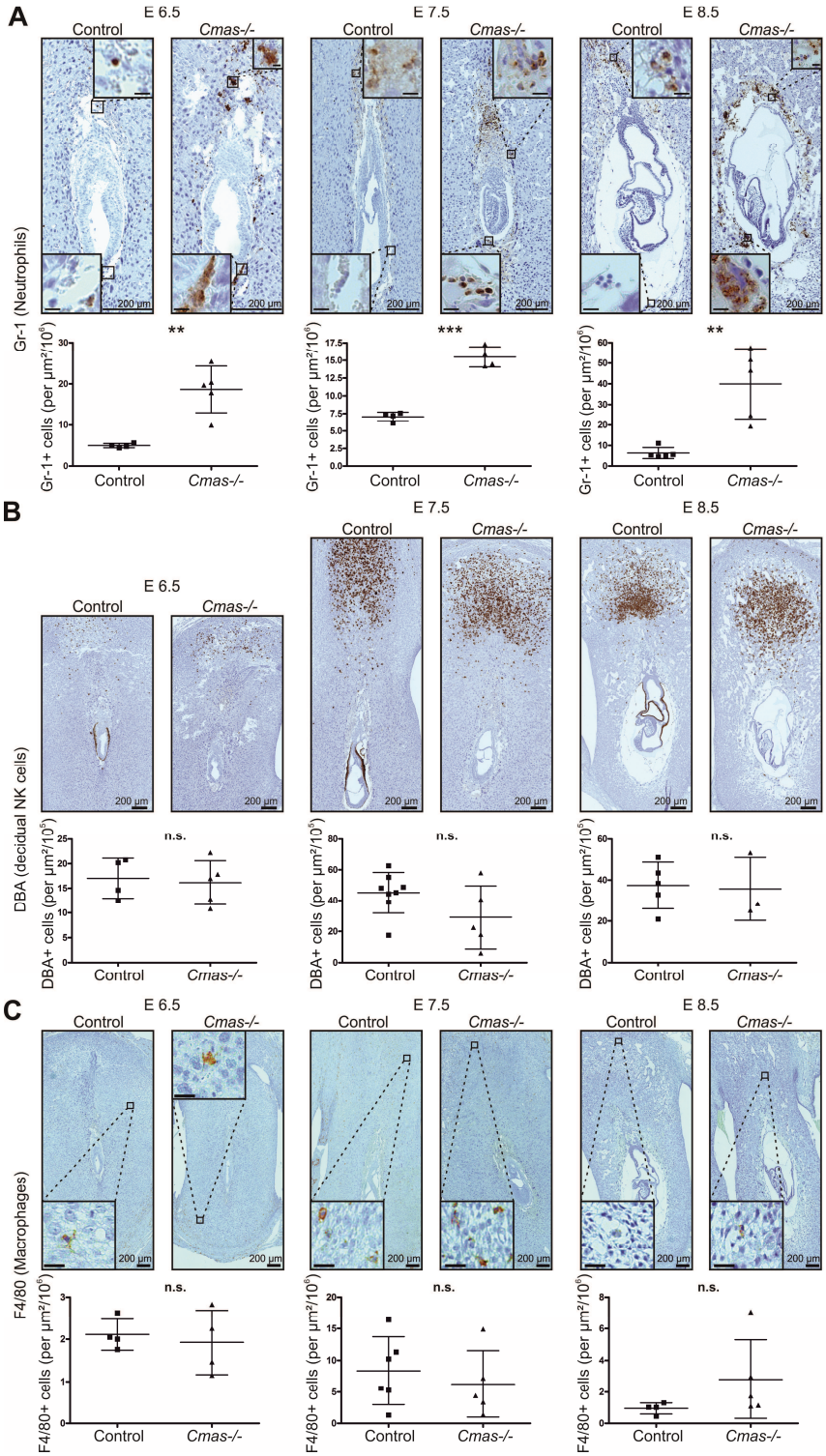

Figure 4. Depletion of maternal neutrophils does not rescue the *Cmas*$^{-/-}$ phenotype. (A) Neutrophils were depleted by intraperitoneal injection of 500 µg anti-Ly6G antibody (1A8, BioXCell) into pregnant mice at E4.5. Ly6G FACS analysis of whole blood from untreated and anti-Ly6G injected pregnant mice at day E8.5. **(B)** Ly6G (neutrophils) immunohistochemical staining of sagittal paraffin sections of embryos within the uterus. Pregnant females were either treated with the isotype antibody (2A3, BioXCell) as a negative control or with anti-Ly6G for neutrophil depletion. Representative images of control (n=6) and *Cmas*$^{-/-}$ (n=4) embryos. **(C)** Mean fetal size of control and *Cmas*$^{-/-}$ embryos from anti-Ly6G treated mother mice as measured by the sum of the areas of amniotic cavity, exocoelomic cavity, ectoplacental cavity and embryo proper in (µm²/10^5) (control n=6, *Cmas*$^{-/-}$ n=4). Schematic overview of measured areas, see Figure S5. Error bars indicate SD. Statistical analyses were performed by Student's t-test. (**P < 0.01). **(D)** Immunohistochemical detection of Cytokeratin-8 to visualise trophoblast cells on sagittal paraffin sections of E8.5 uteri from Ly6G treated mother mice. Representative images of control (n=6) and *Cmas*$^{-/-}$ (n=4) embryos. **(E)** Collagen IV indirect immunofluorescence staining on sagittal paraffin sections of uteri at E8.5 from Ly6G treated mother mice to visualise Reichert's membrane (arrow) and parietal endoderm (arrowheads). Representative images of control (n=6) and *Cmas*$^{-/-}$(n=4) embryos. Nuclei stained with DAPI are shown in white.

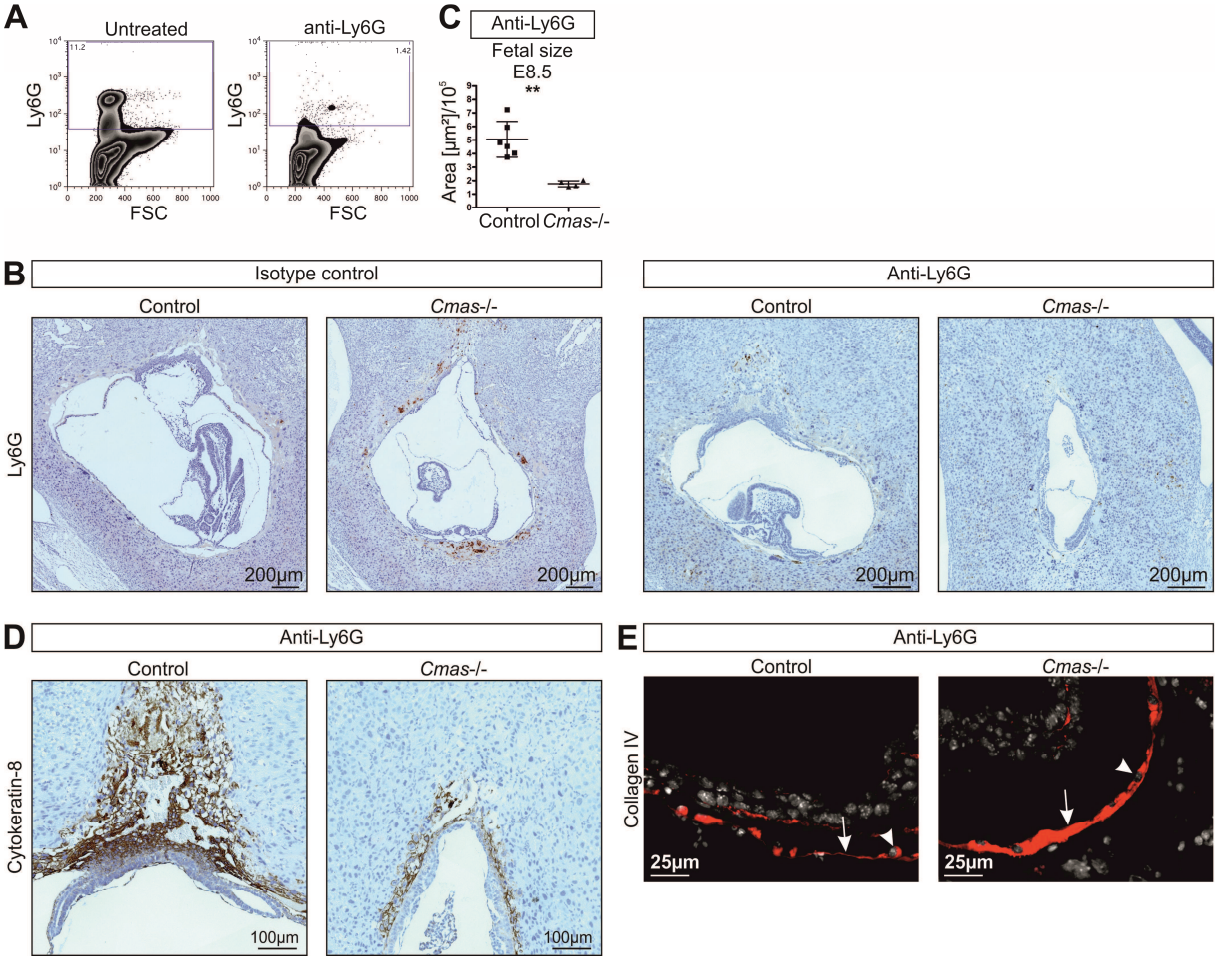

Figure 5. *Cmas*$^{-/-}$ trophoblast cells exhibit increased deposition of complement component 3 (C3). (A) C3 immunohistochemical staining of sagittal paraffin sections of uteri at E8.5. Insets show TGCs. Scale bars in the insets: 25 µm. C3 staining of visceral endoderm (arrowhead) was observed only in control embryos. Representative images of control (n=16) and *Cmas*$^{-/-}$ (n=6) embryos within the uterus. **(B)** C3 immunohistochemical staining of sagittal paraffin sections of uteri at E8.5 from anti-Ly6g treated mother mice. Insets show TGCs without C3 staining on control tissue but extensive staining at TGC cell surface. Representative images of control (n=6) and *Cmas*$^{-/}$ (n=4) embryos within the uterus. Scale bars in the insets: 50 µm.

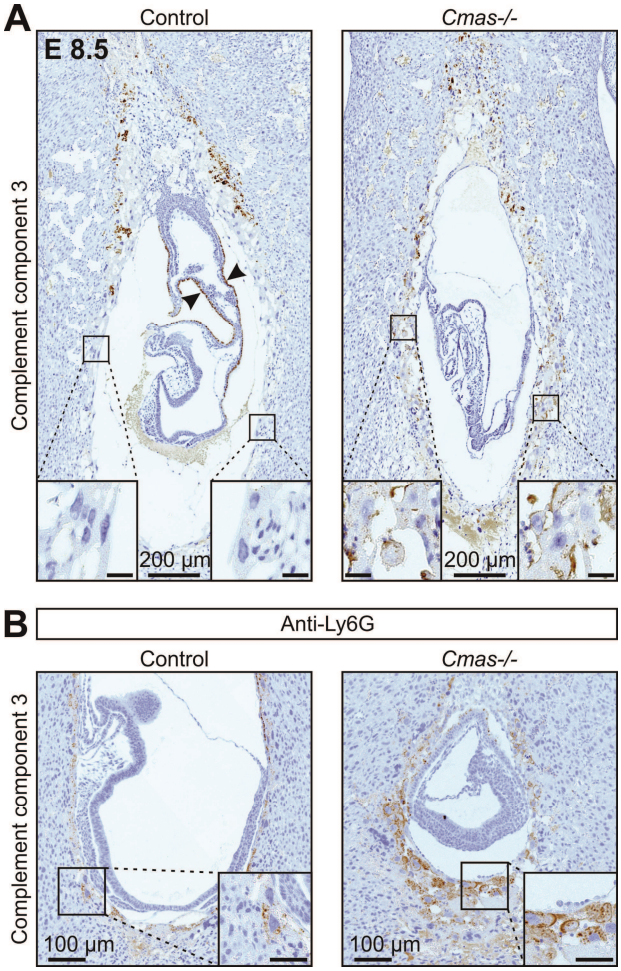

Figure 6. Cobra venom factor (CVF) decomplements the maternal serum and rescues the inflammatory phenotype of *Cmas*$^{-/-}$ implants. (A) C3 Western Blot analysis. Serum of PBS or CVF treated pregnant mice at E8.5 was separated by SDS-PAGE and immunostained with anti-C3 antibody. C3 protein was only detectable in PBS treated mice but depleted in CVF treated pregnant mice. Anti-albumin staining as loading control. **(B)** C3 immunohistochemical staining of sagittal paraffin sections of E8.5 embryos within the uterus of PBS or CVF treated mice. In PBS treated mothers, C3 reactivity was restricted to the EPC in control implants, but was expanded to the entire fetal-maternal interface in *Cmas*$^{-/-}$ embryos with strong staining at the surface of TGCs. In implants of CVF treated mothers the C3 reactivity was abolished irrespective of the genotype. Insets show fetal TGCs. **(C)** Ly6G immunohistochemical staining for neutrophils on sagittal paraffin sections of E8.5 uteri from PBS or CVF treated mice. Ly6G positive cells are sparsely distributed in proximity of control embryos of PBS treated mothers. In contrast, the entire fetal-maternal boundary of *Cmas*$^{-/-}$ implants is infiltrated with Ly6G positive cells in PBS treated mice. CVF treatment does not change the phenotype of controls but reverts Ly6G staining of *Cmas*$^{-/-}$ implants to controls. **(D)** Quantification of Ly6G positive cells (neutrophils) on sagittal paraffin sections of E8.5 uteri of PBS or CVF treated pregnant mice. Error bars indicate SD. Statistical analyses were performed by ANOVA with Newman-Keuls post-test (***P < 0.001). Representative images of experiments of three PBS treated pregnant mice with n=5 control and n=3 *Cmas*$^{-/-}$ embryos, and of three CVF treated pregnant mice with n=5 control and n=4 *Cmas*$^{-/-}$ embryos **(B-D)**.

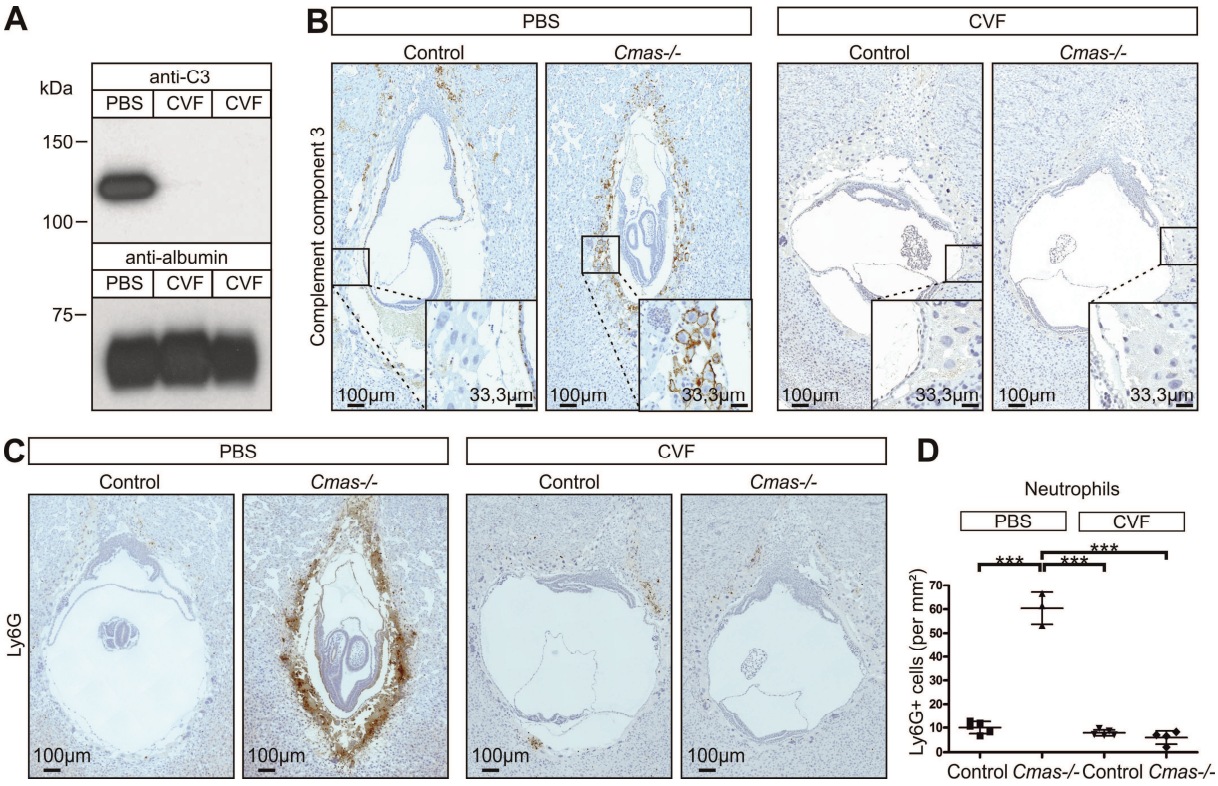

Figure 7. Maternal decomplementation rescues defects in extraembryonic tissues and growth restriction of *Cmas*$^{-/-}$ mice. Pregnant *Cmas*$^{+/-}$ mice were treated at E4.5 and E6.5 either with PBS (n=3) or CVF (n=3) to deplete maternal C3. E8.5 sagittal uteri paraffin sections (**A, B**). **(A)** The reduced size of the ectoplacental cone (EPC) and lack of a chorionic plate (CP) in *Cmas*$^{-/-}$ embryos of PBS treated mothers was reverted to control phenotype upon CVF treatment as visualized by immunohistochemical Cytokeratin-8 staining. The lack of Cebpb reactivity (indirect immunofluorescence) in *Cmas*$^{-/-}$ embryos of PBS treated mothers was restored upon CVF treatment. PNA reactivity documenting the loss of cell surface sialylation was maintained in *Cmas*$^{-/-}$ embryos of PBS as well as of CVF treated mothers, indicating that the asialo-phenotype was not influenced by CVF. Representative images of experiments with PBS treated mice: control n=5, *Cmas*$^{-/-}$ n = 3 embryos; CVF treated mice: control n = 5, *Cmas*$^{-/-}$ n = 4 embryos. **(B)** Collagen IV indirect immunofluorescence (red). Thickened Reichert's membrane (arrow) in *Cmas*$^{-/-}$ embryos of PBS treated mothers was converted to control phenotype upon CVF treatment. Parietal endoderm marked by arrowheads. Nuclei shown in white were stained with DAPI. **(C)** Quantification of Reichert's membrane thickness measured on Collagen IV immunofluorescences at the anti-mesometrial pole (PBS: control n = 6; *Cmas*$^{-/-}$ n = 3 embryos; CVF: control n = 5; *Cmas*$^{-/-}$ n = 4 embryos). **(D)** Mean of fetal size as measured by the sum of areas of amniotic cavity, exocoelomic cavity, ectoplacental cavity and embryo proper in ($\mu m^2/10^5$) (PBS: control n=5; *Cmas*$^{-/-}$ n=4 embryos; CVF: control n=5; *Cmas*$^{-/-}$ n=3 embryos); a scheme of the areas is shown in Figure S5. Statistical analyses by ANOVA with Newman-Keuls post-test (*P < 0.05, **P < 0.01, ***p < 0.001). Error bars indicate SD **(C, D)**.

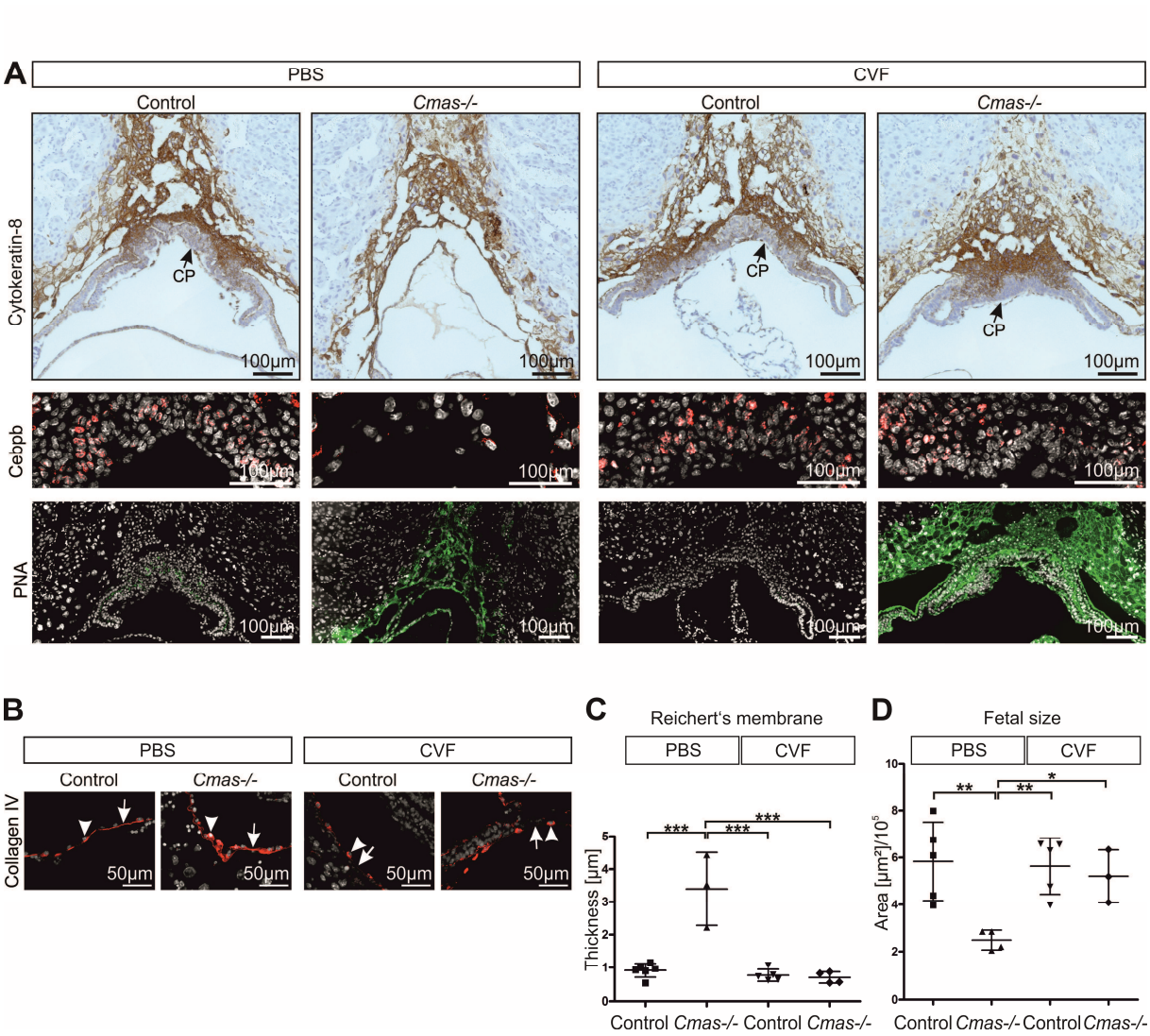

Figure 8. *Cmas*$^{-/-}$ trophoblast cells activate the alternative pathway. Immunohistochemical analyses of complement components **(A)** C1q, **(B)** C4d, **(C)** Properdin and **(D)** C9 on sagittal paraffin-embedded sections of E8.5 embryos within the uterus. The positive C9 staining in both genotypes (upper insets) most likely reflects C9 in the fluid phase in the lumen of decidual blood vessels. Scale bars in all insets: 20 µm. All shown experiments are representative images of control (n=12) and *Cmas*$^{-/-}$ (n=3) embryos.